Spintronic detection of interfacial magnetic switching in a paramagnetic thin film of tris(8-hydroxyquinoline)iron(III)

Dali Sun, Christopher M. Kareis, Kipp J. van Schooten, Wei Jiang, Gene Siegel, Marzieh Kavand, Royce A. Davidson, William W. Shum, Chuang Zhang, Haoliang Liu, Ashutosh Tiwari, Christoph Boehme, Feng Liu, Peter W. Stephens, Joel S. Miller, and Z. Valy Vardeny

Phys. Rev. B **95**, 054423 — Published 17 February 2017

DOI: 10.1103/PhysRevB.95.054423

Spintronics Detection of Interfacial Magnetic Switching in a Paramagnetic Tris(8-hydroxyquinoline)iron(III) Thin Film

Dali Sun[1], Christopher M. Kareis[2] , Kipp J. van Schooten[1], Wei Jiang[3], Gene Siegel[3], Marzieh Kavand[1], Royce A. Davidson[2], William W. Shum[2], Chuang Zhang[1], Haoliang Liu[1], Ashutosh Tiwari[3], Christoph Boehme[1], Feng Liu[3], Peter W. Stephens,[4] Joel S. Miller[2], Z. Valy Vardeny[1,*]

[1]*Department of Physics & Astronomy, University of Utah, Salt Lake City, Utah, 84112.*

[2]*Department of Chemistry, University of Utah, Salt Lake City, Utah, 84112*

[3]*Department of Material Science & Engineering, University of Utah, Salt Lake City, Utah 84112.*

[4]*Department of Physics & Astronomy, Stony Brook University, Stony Brook, NY 11794.*

Organic semiconductors find increasing importance in spin transport devices due to the modulation and control of their properties through chemical synthetic versatility. The organic materials have been used as interlayers between two ferromagnet (FM) electrodes in organic spin valves, as well as for magnetic spin manipulation of metal-organic complexes at the molecular level. In the latter, the substrate-induced magnetic switching in a paramagnetic molecule has been evoked extensively, but studied by delicate surface spectroscopies. Here we present evidence of the substantial magnetic switching in a thin film of the paramagnetic molecule, tris(8-hydroxyquinoline)iron(III) (Feq_3) deposited on a FM substrate, using the magnetoresistance response of electrical 'spin-injection' in an organic spin valve structure, as well as the inverse-spin-Hall effect induced by state-of-art pulsed microwave 'spin-pumping'. We show that interfacial spin control at the molecular level may lead to a macroscopic organic spin transport device; thus, bridging the gap between organic spintronics and molecular spintronics.

*To whom correspondence should be addressed: val@physics.utah.edu

PACS numbers: 85.65.+h, 33.15.Kr, 85.75.-d, 72.25.Pn, 85.75.Bb.

I. INTRODUCTION

Organic semiconductors (OSEC) have attracted intense attention for potential applications in spintronic-based devices because of the long spin relaxation time obtained for spin ½ carriers [1-3]. To date organic spintronics research has focused on the physics of the spin injection and spin transport through the organic interlayer in organic spin valve (OSV) devices. Detection of spin transport through the OSEC layer has been done through a variety of techniques that include magneto-transport [3-12], inverse spin Hall effect (ISHE) [13,14], muon spin rotation [15,16], and two-photon photoemission [17-19]. In most applications the spin control in the device has been achieved via the injected spin-aligned carriers from conventional FM electrodes into the OSEC interlayer, in spite of the conductivity mismatch at their interface that poses a formidable barrier for spin injection [20].

In contrast to organic spintronics, 'molecular spintronics' utilizes the chemical versatility of molecules; in particular those that have paramagnetic metal ions, for manipulating the spin states [21-29]. One particularly promising class of building blocks for molecular spintronics devices is the metalloporphyrins, which exhibit an intrinsic remnant magnetization when in contact with a FM metallic electrode [24], similar to single molecule magnets [30]. Recently, metallophthalocyanines (e.g. CuPc [28], MnPc [31]) also have been intensely studied due to their potential highly spin polarized surface spins ('spinterface') that can act as a spin filter. However, the spin orientation of the molecular ensemble, which is crucial to the ability of spin filtering, was only investigated in the limit of monolayer using a variety of surface science techniques [24-32].

Here we report a spin current-based detection scheme of a molecular spin ensemble by incorporating the paramagnetic semiconductor tris(8-hydroxyquinoline)iron [33] (Feq_3; shown in Figure. 1a and S. I. Fig. S1-S3) as an interlayer into two macroscopic spintronic devices: (i) a FM/Feq_3/Au trilayer configuration ('OSV-like' device) using magnetoresistance response from electrically injected spin aligned carriers; and (ii) a FM/ Feq_3/Pt trilayer configuration for ISHE response using microwave (MW) pumped pure spin current. The Feq_3 layer in the OSV-like device functions as a spin filter; but, surprisingly it also exhibits a 'switching field' that mimics the coercive field of a conventional FM film. Consequently, the device magnetoresistance

response, MR(B) shows similar features as that of a more conventional OSV device. Using SQUID magnetometry we verified the substantial magnetic ordering and switching that occur in the Feq_3 layer, which is attributed to an indirect antiferromagnetic (AFM) exchange interaction with the FM metallic electrode in the device. Due to this AFM exchange the NiFe/Feq_3 layer in an ISHE device generates a pure spin current having an *opposite* direction of spin polarization to the magnetization of the NiFe substrate, which results in an ISHE response of reverse polarity compared to that of a NiFe/Pt bilayer. Our experimental findings are further supported by first-principles DFT-type calculations.

II. EXPERIMENTAL DETAILS

Compared to the more conventional diamagnetic tris(8-hydroxyquinoline)aluminum (Alq_3), which has been widely used as OSEC interlayer in OSV devices [4], Feq_3 has *five electron spins* that originate from the 3d transition metal Fe^{III} ion [33] (Fig. 1a inset and S. I. Fig. S1). Therefore the ground state spin quantum number is S=5/2 [34]. The Feq_3 film is an air-stable semiconductor with an energy gap in the near-IR spectral range that results in photoluminescence emission at ~1.65 eV (~750 nm) (Fig. 1a). Also the film exhibits paramagnetic Curie-Weiss susceptibility behavior ($\chi \propto 1/T$) with no detectable hysteresis (Fig. 1b). A schematic structure of the OSV-like device based on a Feq_3 interlayer is illustrated in Fig. 2a. The device consists of a bottom FM metallic electrode, Feq_3 interlayer film (that was grown *in situ* by thermal evaporation), and capped with a nonmagnetic Au top electrode; a magnetic field, $\boldsymbol{B}$ is applied parallel to the device substrate. For the ISHE measurements the Au cap electrode is replaced by Pt metal film, which, due to its large spin-orbit coupling is used for detecting spin currents.

We fabricated the OSV-type devices on two types of bottom FM electrodes. One is half-metal FM $La_{0.67}Sr_{0.33}MnO_3$ thin film that was epitaxially grown on $SrTiO_3$ substrates by pulsed laser deposition; and fabricated for bottom electrode using conventional wet-etch optical lithography. Another is the $Ni_{80}Fe_{20}$ bottom electrode that was grown by e-beam evaporation through a shadow mask on Si_3N_4 (400 nm)/Si substrates in a vacuum chamber devoted for metal deposition. The FM electrodes were subsequently transferred without breaking the vacuum into a second

chamber devoted to OSEC deposition. The Alq_3 (Aldrich) and Feq_3 (synthesized by literature method [33]) films were grown *in situ* by thermal evaporation. The fabricated structures were transferred back to the metal deposition chamber for e-beam evaporation of an Au top electrode (25 nm) in a crossbar configuration. Typical device area was ~ 200 × 500 μm.

For an ISHE-type device, an Al thin film electrode (150 nm) was firstly grown on a glass template (3×50 mm) by sputtering using conventional optical lithography. Subsequently two Cu contacts (30 nm thick) with a gap of 3 mm (extended from an Al bottom electrode) were grown by e-beam evaporation through a shadow mask, followed by a strip of Pt electrode (3.5 mm × 1 mm × 7 nm). Without breaking the vacuum, the fabricated structures were transferred with another shadow mask to the organic deposition chamber for OSEC deposition. The OSEC deposition was similar to that used for the OSV-like device. Then ferromagnetic layer ($Ni_{80}Fe_{20}$, 15 nm), SiO_2 (500 nm) dielectric layer and top Cu thin film (30 nm) were all grown in series on the OSEC layer by e-beam evaporation through a shadow mask on the OSEC materials.

Transport measurements performed using a Quantum Design Physical Property Measurement System (PPMS-9) combined with a Keithley 2400 source meter. The magnetic field, B, was applied parallel to the device substrate. The MR is defined as: $MR(B) = (R(B) - R(0))/R(0)$, where $R(0)$ is the junction resistance at $B = 0$, and $R(B)$ is the resistance measured at field B using the four-points method. The magnetization measurements for the susceptibility and devices were performed using the Quantum Design MPMS-5 5 T superconducting quantum interference device (SQUID) magnetometer. The p-ISHE measurements were carried out at room temperature in a Bruker ElexSys E580 X-band (~9.7 GHz) pulsed EPR spectrometer equipped with a dielectric resonator (Bruker FlexLine ER 4118 X-MD5). The MW pulse duration time was set to 2 μs at a repetition rate of 500 Hz. The maximum pulsed MW power was ~1 kW resulting in an excitation field amplitude B_1=1.1 mT at the sample location. The p-ISHE(B) response measurements and time dynamics required averaging over 10240 shots. First-principles calculations were carried out using local spin density approximation (LSDA) with onsite Coulomb interactions and projector augmented-wave method in Vienna ab-initio simulation package (VASP) based on density functional theory, in which an additional on-site Hubbard-U

term is included on the iron(III) (U=6.0 eV, J=0.9 eV). The DFT-D2 method [34] was applied to describe the van der Waals interactions that may influence molecular absorption and geometries.

II. RESULTS AND DISCUSSION

A. Magnetoresistance measurements

Typical MR(B) responses of various OSV-like FM/Feq_3 devices with various FM substrates are presented in Figs. 2b-2c. The MR(B) response of the NiFe/Feq_3 device has two different response components. The jump of ~0.2% is observed when the FM substrate magnetization switches at the coercive field, $B_{C1} \approx 3$ mT. This is due to the anisotropic MR(B) response of the NiFe electrode (see S. I. Fig. S4). The broad negative response of ~ 0.1% is due to MR(B) due to spin current through the device. The maximum MR(B) value, MR_{max}, obtained in this OSV-like device is comparable to NiFe-based conventional OSV devices [15,16]. Surprisingly we observed that the MR(B) response switches back to the low resistance state at B=B_{C2} ~50 mT, showing a similar response to that observed in conventional OSV, although only a single FM electrode is used here as opposed to two FM electrodes in more traditional OSV devices. This indicates that an unusual magnetic ordering occurs in the Feq_3 layer when it is placed near a FM substrate, which is modulated by the external field. As a control experiment, upon replacing the bottom NiFe electrode by an Au electrode to form an Au/Feq_3/Au diode, no MR response was obtained (S. I. Fig. S5). This excludes the possibility that the MR(B) response here is caused by the organic MR (OMAR) [35] or δB mechanism in the Feq_3 layer [36].

When replacing the bottom NiFe electrode by LSMO which is half-metal FM (see S. I. Fig. S6 for I-V characteristics), which has ~100% spin aligned carrier injection capability [37], then the obtained MR_{max} (after the non-hysteresis linear MR(B) response that originates from the LSMO electrode [38] was subtracted out; S. I. Fig. S7) is enhanced by an order of magnitude reaching ~5.4% (Fig. 2c), and the switching field, B_{C2} increases to ~100 mT. The larger MR_{max} observed for the LSMO-based OSV-like device indicates that spin aligned carrier injection into the OSEC interlayer has occurred, consistent with the different abilities of NiFe and LSMO FM electrodes to inject spin aligned carriers into an OSEC. The Coulomb blockade induced magnetoresistance

cannot explain our observations either, since it usually occurs at very low temperature (below 1 K) [40]. We note that the MR response in LSMO-based device has opposite polarity compared to that of NiFe-based device. This may be due to the interaction of the Feq_3 molecules and FM electrode at the interface caused by the relative alignment of the Feq_3 HOMO/LUMO and the FM electrode's Fermi level [12].

We also measured the MR(B) response in both NiFe and LSMO-based OSV-like devices at different temperatures, T. MR_{max} vs. T for these devices is summarized in Fig. 2d. Similar to conventional OSV devices [4], MR_{max} decreases steeply with increasing T and vanishes at 100 K for the LSMO-based OSV-like devices. In contrast, the MR response in the NiFe/Feq_3/Au device survives up to 200 K. We conclude from the various MR(B) and MR_{max} responses vs. temperature and voltage (S. I. Fig. S9) that the OSV-like devices based on Feq_3 interlayer behave very similar to conventional OSV devices that contain two FM electrodes. Therefore the OSV-like device may be considered as a simplified version of OSV, which is based on a single FM electrode [41,42].

B. Magnetization measurements

At variance with the previously reported FM ordering in metalloporphyrins and metallophthalocyanines monolayer detected by surface science techniques [24-26], a substantial FM ordering of the Feq_3 layer in the OSV-like device configuration was observed using conventional magnetometry 'SQUID' measurements, i.e. $M(B)$ response (Fig. 3), which may explain the OSV-like MR response of FM/Feq3/Au trialyers. First we observed that the $M(B)$ response of a pristine NiFe film (Fig. 3a) shows an abrupt hysteretic response at $B < 2$ mT, consistent with its coercive field, B_{C1}. Next we observed the magnetization response of Feq_3 based structures. Compared to the linear paramagnetic response of pristine Feq_3 film having S=5/2 in the ground state (Fig. 1b), the $M(B)$ loops of NiFe/Feq_3 and LSMO/Feq_3 'OSV-like film structures' clearly show a second hysteretic transition (B_{C2}) at a higher field (Figs. 3b and 3d). This is distinct from the abrupt transition of the NiFe (or LSMO) electrode seen at low field. As a control experiment, M(B) loops of NiFe/Alq_3 and LSMO/Alq_3 exhibit only the M(B) response feature at B_{C1} that originate from the FM substrate (Figs. 3c and 3e). This indicates that the

observed *MR*(B) and *M*(B) response at Bc_2 cannot be attributed to the π orbitals/substrate hybridization from the hydroxyquinoline ligands [18,19,43]. We note that the narrow hysteresis response of the NiFe electrode at ~B_{C1} is broader in the 'OSV-like film structures' than that of the pristine NiFe film. This magnetic 'hardening' originates from the OSEC overlayer, and is consistent with the enhanced exchange interaction found previously for π-conjugated molecules deposited on FM surfaces due to the proximity of the molecules to the FM atoms [44].

The *M*(*B*) responses of NiFe/Feq_3 'OSV-like film structures' measured upon cooling under two different and opposite magnetic fields of +300 mT and -1 T, are shown in Fig. 3f. The *M(B*) response asymmetry with respect to $B = 0$ is seen when the field is swept in one direction and then to the opposite direction. This indicates the presence of a 'magnetic exchange bias' [45-48], which results from an AFM coupling [24] at the interface between the Feq_3 and NiFe layers. We note that π-conjugated nonmagnetic organic molecules deposited on FM metallic film show only a symmetric *M(B)* response [4,12,44]. Re-orientated easy axis on the surface of NiFe/Feq_3 layer from in-plane to out-of-plane can be ruled out because the total magnetization along the in-plane direction is unchanged in opposite field cooling. We conclude that the SQUID magnetometry measurements conclusively reveal that the paramagnetic Feq_3 layer in the proximity of the FM substrate is *magnetically ordered*, consistent with the observed MR(*B*)-type response of the OSV-like devices. The resulting magnetic switching of the remnant field in the Feq_3 layer occurs at $B_{C2} > B_{C1}$, and this generates the OSV-like MR(*B*) response in the OSV-like devices.

C. Inverse Spin-Hall effect measurements

Further evidence for an AF order of the Feq3 layer deposited on a FM substrate is provided by the ISHE. Figure 4a demonstrates the working principle and schematic structure of an ISHE device based on Feq_3 molecules. The magnetization dynamics $\boldsymbol{M}(\mathbf{t})$ under ferromagnetic resonance (FMR) condition induces a pure spin current ($\boldsymbol{J_S}$) in the adjacent non-magnetic Pt layer via spin pumping. Since Pt has a large spin Hall angle ($\theta_{SH} \sim 0.06$) [50], therefore the induced spin current leads to a related electric field, $\boldsymbol{E_{ISHE}}$ perpendicular to both $\boldsymbol{J_S}$ and the spin polarization $\boldsymbol{S}$: namely $\boldsymbol{E_{ISHE}} = \theta_{SH}\boldsymbol{J_S} \times \boldsymbol{S}$. We have used a state-of-the-art pulsed MW excitation [51] to deliver high MW power (~ 1 kW) to the FM substrate that consequently

generates high spin current density in the Pt layer with minimum thermal/resonant heating effect (see S. I. Fig. S11 and Ref. 52). With the pulsed ISHE (p-ISHE) method it is possible to investigate a Spinterface feature that occurs in Feq_3 layer only several molecular monolayers thick.

The inset of Fig. 4b shows the p-ISHE voltage generated from a NiFe/Pt ISHE device without Feq_3, measured at room temperature with an in-plane (i.e. $\boldsymbol{\theta_B}$=0º) field, $\boldsymbol{B}$, as illustrated in Fig. 4a. The p-ISHE response ($\mathbf{V_{ISHE}}$ ~ -1.3 mV at $\boldsymbol{\theta_B}$=0º) is about two orders of magnitude larger than that of the cw-ISHE, due to the high pulsed MW excitation intensity [51]. Possible heating effect can be excluded here since its resulting magnetic field response is independent of the **B** direction, in sharp contrast with the asymmetric p-ISHE response at $\boldsymbol{\theta_B}$=0º and $\boldsymbol{\theta_B}$=180º seen in Fig. 4a [51,52]. When a 7 nm thick Feq_3 layer (~7 monolayers) is inserted in between the NiFe and Pt layers, the observed p-ISHE response from the Pt layer is reduced to ~ 76 μV (Fig. 4c); see also S.I. Fig. S12. Importantly, the p-ISHE polarity (at $\boldsymbol{\theta_B}$=0º and $\boldsymbol{\theta_B}$=180º) is *reversed* (Fig. 4c) compared to the response without the Feq_3 interlayer. The p-ISHE magnitude and polarity would no change if the spin current would be directly generated from the NiFe layer into the Pt layer via pinholes. We thus conclude that the observed p-ISHE(B) response in the NiFe/Feq_3/Pt structure originates from the spin current that is generated into the Pt layer from the Feq_3 layer itself; we note that spin-pumping from a paramagnetic layer was recently demonstrated [52].

Due to the AFM exchange interaction between the NiFe and Feq_3 layer that is manifested in the MR(B) and SQUID measurements, we conclude that the induced Feq_3 magnetization, $\boldsymbol{m}$ is opposite to $\boldsymbol{M}$. Consequently $\boldsymbol{m}$ in the Feq_3 layer precesses in the opposite direction under the influence of the dynamic magnetization $\boldsymbol{M}$(t) in the NiFe layer, thereby generating magnons with opposite spin **S** respect to those in the NiFe layer. The generated magnons, in turn produce spin current at the Feq_3/Pt interface having opposite spin direction to that produced without the Feq_3 layer, and therefore $\boldsymbol{E_{ISHE}}$ in the Pt layer reverses polarity (see right panel in Fig. 4a). We also note that the electron paramagnetic resonance for the paramagnetic Feq_3 molecules measured at the MW frequency that we use here (~9.7 GHz) is ~300 mT (g≈2), which differs substantially from the obtained FMR in the NiFe layer (107 mT) and NiFe/Feq3 bilayer (111mT). We also measured the p-ISHE responses in a trilayer with smaller Feq_3 thickness (~5 nm) (S.I. Fig. S13).

We confirm that the p-ISHE polarity in this device is still reversed compared to the NiFe/Pt device. In addition the p-ISHE response is larger (~93 μV) due to the enhanced exchange coupling at smaller Feq_3 thickness. We therefore conclude that the ISHE measurements provide more direct evidence for a robust AFM exchange interaction between the NiFe and Feq_3 layer, which is consistent with the MR(B) and SQUID measurements in the OSV-like devices.

D. DFT calculation for the interaction between the FM substrate and Feq_3 film

Our conclusion from the measurements above is supported by density functional theory (DFT) electronic-structure calculations for the Feq_3 molecules in intimate contact with a FM substrate. To deduce the magnetic ordering strength within the Feq_3 layer in proximity to the FM substrate, we extract the exchange coupling constant (J_{ex}) among the Feq_3 molecules by fitting the Heisenberg spin lattice model to the DFT-calculated energy difference between FM and AFM states (see S.I. section 12). For a free-standing Feq_3 molecular monolayer (Fig. 5a), the energy difference, ΔE between AFM and FM spin configuration is very small ($\Delta E = E_{AFM} - E_{FM} < 0.1$ meV, the energy convergence criteria is set at 0.1 meV), which translates to a negligible J_{ex} (~ 0.002 meV) ; this indicates a paramagnetic free-standing Feq_3 layer (S. I. Fig. S15). However, when the Feq_3 layer is deposited onto the FM NiFe substrate that forms interface layer (Fig. 5b), ΔE between AFM and FM spin configuration becomes much larger ($\Delta E = E_{AFM} - E_{FM} \sim 8$ meV), and the effective coupling among the Feq_3 molecules changes to strong FM coupling with $J_{ex} \sim 0.8$ meV. This indicates that the paramagnetic Feq_3 layer transitions to weak FM ordering (S. I. Fig. S16a), similar to the Fe-porphyrin layer [24,26]. The origin of FM ordering in the interface Feq_3 can be understood from analysis of the spin-resolved, partial density of state (p-DOS) of the NiFe/Feq_3 system (S. I. Fig. S16b). When the Feq_3 molecules are in close proximity with the NiFe substrate, although there is no direct overlap of Fe^{III} and NiFe *d*-orbitals, there exist Fe-O, Ni-O and Fe-N, Ni-N interactions, as deduced from the spin DOS (S. I. Fig. S16b), which are able to mediate a 'super-exchange'-like interaction. Furthermore, the results of first-principles calculations indicate that interface Feq_3 layer prefers an AFM interface-mediated coupling with the underlying FM NiFe substrate, with an energy difference, ΔE =

($E_{FM} - E_{AFM}$) > 25 meV (S. I. Fig. S16a). This is in agreement with the observed exchange bias in the obtained $M(B)$ response and reversed p-ISHE response (Figs. 3 and 4).

III. SUMMARY

The discovery of versatile spin filter functionality of Feq_3 thin films and its ability to form an OSV-like device is an important advance for organic spintronics applications. We employed two spin-current based detection themes for studying the magnetic order of Feq_3 layer grown on a FM substrate, namely magnetoresistance and ISHE. We showed that both the OSV-like MR(B) and reversed ISHE(B) response originate from the AFM ordering that occurs at the Feq_3/FM interface. Using a variety of chemical synthesis techniques, incorporation of different transition metals (e.g. Mnq_3, Crq_3, etc.) and other ligands or a proper FM substrate should would enable tuning of the FM/OSEC exchange coupling, as well as the degree of magnetic ordering at the molecular level for altering the magnitude of MR(B), ISHE and magnetization responses at the macroscopic level.

Acknowledgments

This work was supported by the National Science Foundation-Material Science & Engineering Center (NSF-MRSEC; DMR-1121252). The ISHE measurements were supported by the National Science Foundation (DMR-1404634). Use of the National Synchrotron Light Source, Brookhaven National Laboratory was supported by the DOE BES (DE-AC02-98CH10886).

Additional information

Supplementary Information is available in the online version of the paper.

The authors declare no competing financial interests.

*Correspondence and requests for materials should be addressed to Z.V.V. (val@physics.utah.edu).

References:

1. V. A. Dediu, L. E. Hueso, I. Bergenti, and C. Taliani, Spin routes in organic semiconductors. *Nat. Mater.* **8,** 707–716 (2009).
2. D. Sun, E. Ehrenfreund, and Z. V. Vardeny, The first decade of organic spintronics research. *Chem. Comm.* **50**, 1781-1793 (2013).
3. S. Pramanik, et al. Observation of extremely long spin relaxation times in an organic nanowire spin valve. *Nat. Nanotech.* **2**, 216-219 (2007).
4. Z. H. Xiong, D. Wu, Z. V. Vardeny, and J. Shi, Giant magnetoresistance in organic spin-valves. *Nature* **427**, 821–824 (2004).
5. J. W. Yoo et al. Spin injection/detection using an organic-based magnetic semiconductor. *Nat. Mater.* **9**, 638-642 (2010).
6. T. D. Nguyen et al. Isotope effect in spin response of π-conjugated polymer films and devices. *Nat. Mater*. **9**, 345–352 (2010).
7. D. Sun, et al. Giant Magnetoresistance in organic spin valves. *Phys*. *Rev*. *Lett*. **104**, 236602 (2010).
8. T. S. Santos et al. Room-Temperature Tunnel magnetoresistance and spin-polarized tunneling through an organic semiconductor barrier. *Phys*. *Rev*. *Lett*. **98**, 16601 (2007).
9. C. Barraud, et al. Unraveling the role of the interface for spin injection into organic semiconductors. *Nat*. *Phys*. **6**, 615–620 (2010).
10. S. Sanvito, Molecular spintronics: The rise of spinterface science. *Nat*. *Phys*. **6**, 562–564 (2010).
11. M. Galbiati, Spinterface: Crafting spintronics at the molecular scale. *MRS* Bulletin, **39**, 602 (2014)
12. D. Sun, et al, Active control of magnetoresistance of organic spin valves using ferroelectricity. *Nat. Commun*. **5**, 4396 (2014).
13. K. Ando, S. Watanabe, S. Mooser, E. Saitoh and H. Sirringhaus, Solution-processed organic spin-charge converter. *Nat*. *Mater*. **12**, 622-627 (2013).
14. S. Watanabe, et al. Polaron spin current transport in organic semiconductors. *Nat*. *Phys*. **10**, 308-313 (2014).

15. A. J. Drew, et al. Direct measurement of the electronic spin diffusion length in a fully functional organic spin valve by low-energy muon spin rotation. *Nat*. *Mater*. **8**, 109–114 (2009).
16. L. Schulz et al. Engineering spin propagation across a hybrid organic/inorganic interface using a polar layer. *Nat*. *Mater*. **10**, 39–44 (2011).
17. M. Cinchetti et al. Determination of spin injection and transport in a ferromagnet/organic semiconductor heterojunction by two-photon photoemission. *Nat*. *Mater*. **8**, 115–119 (2009).
18. S. Steil et al. Spin-dependent trapping of electrons at spinterfaces. *Nat. Phys*. **9**, 242-247 (2013).
19. A. Droghetti, et al. Electronic and magnetic properties of the interface between metal-quinoline molecules and cobalt. *Phys. Rev. B* **89**, 094412 (2014).
20. G. Schmidt, D. Ferrand, L. W. Molenkamp, A. T. Filip and B. J. van Wees, Fundamental obstacle for electrical spin injection from a ferromagnetic metal into a diffusive semiconductor. *Phys*. *Rev*. *B* **62**, R4790 (2000).
21. A. R. Rocha et al. Towards molecular spintronics. *Nat. Mater*. **4**, 335-339 (2005).
22. S. Sanvito, Molecular spintronics. *Chem. Soc. Rev.* **40**, 3336–3355 (2011).
23. S. Sanvito, Organic spintronics: Filtering spins with molecules. *Nat. Mater*. **10**, 484-485 (2011)
24. H. Wende et al. Substrate-induced magnetic ordering and switching of iron porphyrin molecules. *Nat. Mater.* **6**, 516-520 (2007).
25. P. Gambardella et al. Supramolecular control of the magnetic anisotropy in two-dimensional high-spin Fe arrays at a metal interface. *Nat. Mater*. **8**, 189-193 (2009).
26. M. Mannini et al. Magnetic memory of a single-molecule quantum magnet wired to a gold surface. *Nat. Mater*. **8**, 194-197 (2009).
27. A. L. Rizzini et al. Coupling single molecule magnets to ferromagnetic substrates. *Phys. Rev. Lett*. **107**, 177205 (2011)
28. M. Warner et al. Potential for spin-based information processing in a thin-film molecular semiconductor. *Nature* **503**, 504-508 (2013).
29. T. Miyamachi et al. Robust spin crossover and memristance across a single molecule. *Nat. Commun*. **3**, 938, (2012).

30. L. Bogani and W. Wernsdorfer, Molecular spintronics using single-molecule magnets. *Nat. Mater*. **7**, 179-186 (2008).
31. F. Djeghloul et al. Direct observation of a highly spin-polarized organic spinterface at room temperature. *Sci. Rep.* **3**, 1272 (2013).
32. S. Schmaus et al. Giant magnetoresistance through a single molecule. *Nat. Nanotech.* **6**, 185-189 (2011).
33. J. E. Tackett and D. T. Sawyer, Properties and infrared spectra in the potassium bromide region of 8-quinolinol and its metal chelates. *Inorg. Chem.* **3**, 692-696 (1964).
34. W. Jiang et al. Structural, electronic, and magnetic properties of tris(8-hydroxyquinoline)iron(III) molecules and its magnetic coupling with ferromagnetic surface: first-principles study. J. Phys.: Condens. Matter. **28**, 176004 (2016).
35. Ö. Mermer et al. Large magnetoresistance in nonmagnetic π-conjugated semiconductor thin film devices. *Phys. Rev. B* **72**, 205202 (2005).
36. M. Cox, S. P. Kersten, J. M. Veerhoek, P. Bobbert, and B. Koopmans. ΔB mechanism for fringe-field organic magnetoresistance. *Phys. Rev. B* **91**, 165205 (2015).
37. J.-H. Park, et al. Direct evidence for a half-metallic ferromagnet. *Nature* 392, 794–796 (1998).
38. D. Wu, Z. Xiong, X. Li, Z. V. Vardeny and J. Shi, Magnetic-field-dependent carrier injection at $La_{2/3}Sr_{1/3}MnO_3$ and organic semiconductors interfaces. *Phys. Rev. Lett*. **95**, 016802 (2005)
39. M. Grünewald et al. Tunneling anisotropic magnetoresistance in organic spin valves. *Phys. Rev. B* **84**, 125208 (2011).
40. M. Urdampilleta, S. Klyatskaya, J. P. Cleuziou, M. Ruben and W. Wernsdorfer, Supramolecular spin valves. *Nat. Mater.* **10**, 502-506 (2011).
41. K. V. Raman et al. Interface-engineered templates for molecular spin memory devices. *Nature* **493**, 509-513 (2013).
42. K. V. Raman, Interface-assisted molecular spintronics. Interface-assisted molecular spintronics. *Appl. Phys. Rev*. **1**, 031101 (2014).
43. Y. Zhan et al, Efficient Spin Injection Through Exchange Coupling at Organic Semiconductor/Ferromagnet Heterojunctions. *Adv. Mater.* **22**, 1626–1630 (2010).

44. M. Callsen, V. Caciuc, N. Kiselev, N. Atodiresei and S. Blügel, Magnetic hardening induced by nonmagnetic organic molecules. *Phys. Rev. Lett.* **111**, 106805 (2013)
45. J. Nogués, and I. K. Schuller, Exchange bias. *J. Magn. Magn. Mater.* **192**, 203-232 (1999).
46. J. Hong, T. Leo, D. J. Smith, and A. Berkowitz, E. Enhancing exchange bias with diluted antiferromagnets. *Phys. Rev. Lett.* **96**, 117204 (2006).
47. M. Gruber et al. Exchange bias and room-temperature magnetic order in molecular layers. *Nat. Mater*. **14**, 981–984 (2015).
48. C. Nistor et al, Exchange bias of TbPc2 molecular magnets on antiferromagnetic FeMn and ferromagnetic Fe films. *Phys. Rev B* **92**, 184402 (2015).
49. K. Ando et al. Electrically tunable spin injector free from the impedance mismatch problem. *Nat. Mater*. **10**, 655-659 (2011).
50. J. C. Rojas-Sánchez et al. Spin Pumping and Inverse Spin Hall Effect in Platinum: The Essential Role of Spin-Memory Loss at Metallic Interfaces. *Phys. Rev. Lett.* **112**, 106602 (2014).
51. D. Sun, et al. Inverse Spin Hall Effect from pulsed Spin Current in Organic Semiconductors with Tunable Spin-Orbit Coupling. *Nat. Mater.* (2016). doi:10.1038/nmat4618.
52. K. Ando and E. Saitoh, Observation of the inverse spin Hall effect in silicon. *Nat. Commun*. **3**, 629 (2012).
53. Y. Shiomi and E. Saitoh, Paramagnetic Spin Pumping. *Phys. Rev. Lett.* **113**, 266602 (2014).

Figure Captions:

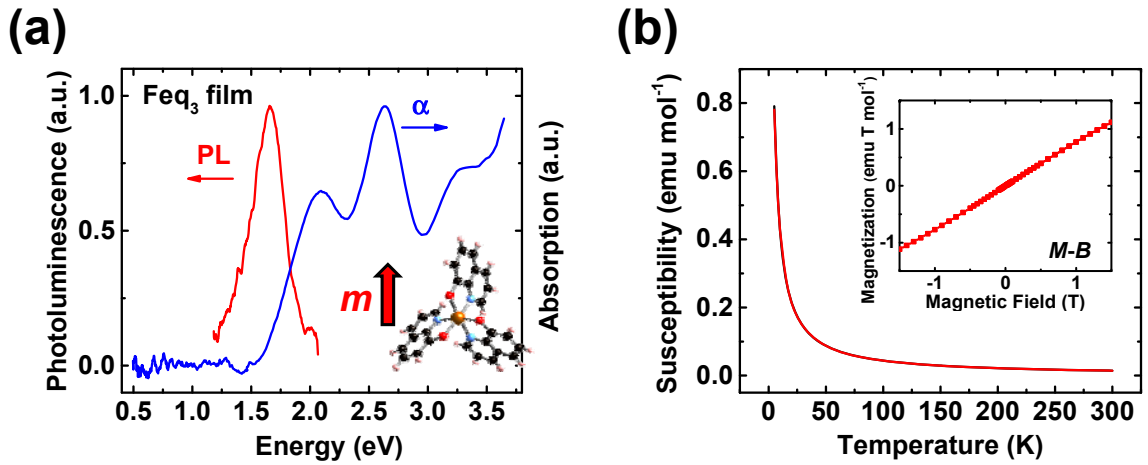

FIG. 1. (Color online) Feq_3 film properties and basic device characterization. (a) Absorption and photoluminescence spectra of an evaporated Feq_3 thin film on quartz substrate. The inset shows the molecular structure of Feq_3 that contains a Fe^{III} ion having spin, S=5/2 (see also S. I. Fig. S1). (b) Magnetic susceptibility of a Feq_3 pristine film on quartz as a function of temperature, T, measured by SQUID magnetometer. The inset shows that the resultant $M(B)$ response is characteristic of paramagnetic behaviour.

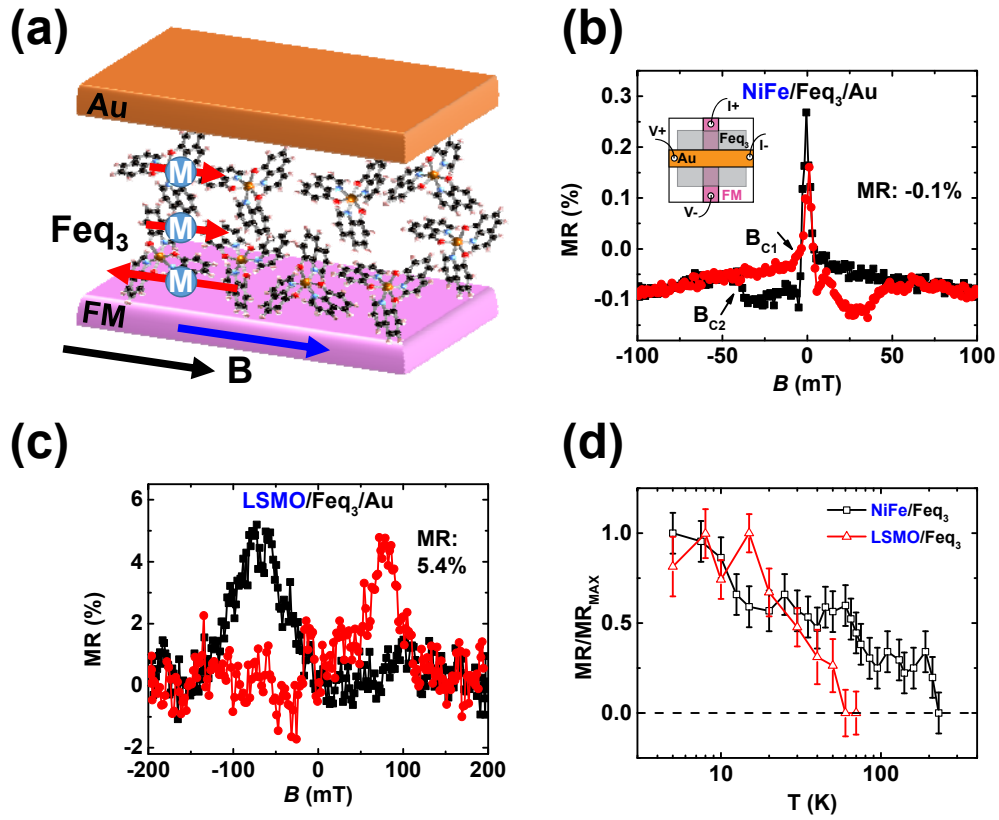

FIG. 2. (Color online) MR(*B*) response of various 'OSV-like' devices having a single FM electrode achieved via electrical spin-injection from the FM electrode. (a) Schematic structure of an 'OSV-like' device that consists of a FM bottom electrode, organic spin filter layer (Feq_3), and capped with a nonmagnetic Au electrode. The external magnetic field ***B*** is applied parallel to the film. Spin aligned carriers of both spin orientations are injected from the FM electrode and undergo spin filtering by the Feq_3 layer (where one spin orientation is filtered) before reaching the Au electrode. At the interface Feq_3 molecules present an opposite magnetic ordering respect to the bottom FM electrode. The blue arrow indicates the magnetization direction in the FM electrode. (b) and (c), Typical MR(*B*) responses of NiFe-based and LSMO-based 'OSV-like' devices at 5K, respectively, with the same Feq_3 spacer thickness (50 nm). B_{C1} and B_{C2} indicate the switching field of the bottom FM electrode and Feq_3 layer, respectively. The inset of (b) illustrates the device geometry for MR measurements. (d) MR_{max} of NiFe and LSMO-based OSV-like devices vs. temperature, normalized to MR_{max} at 5K.

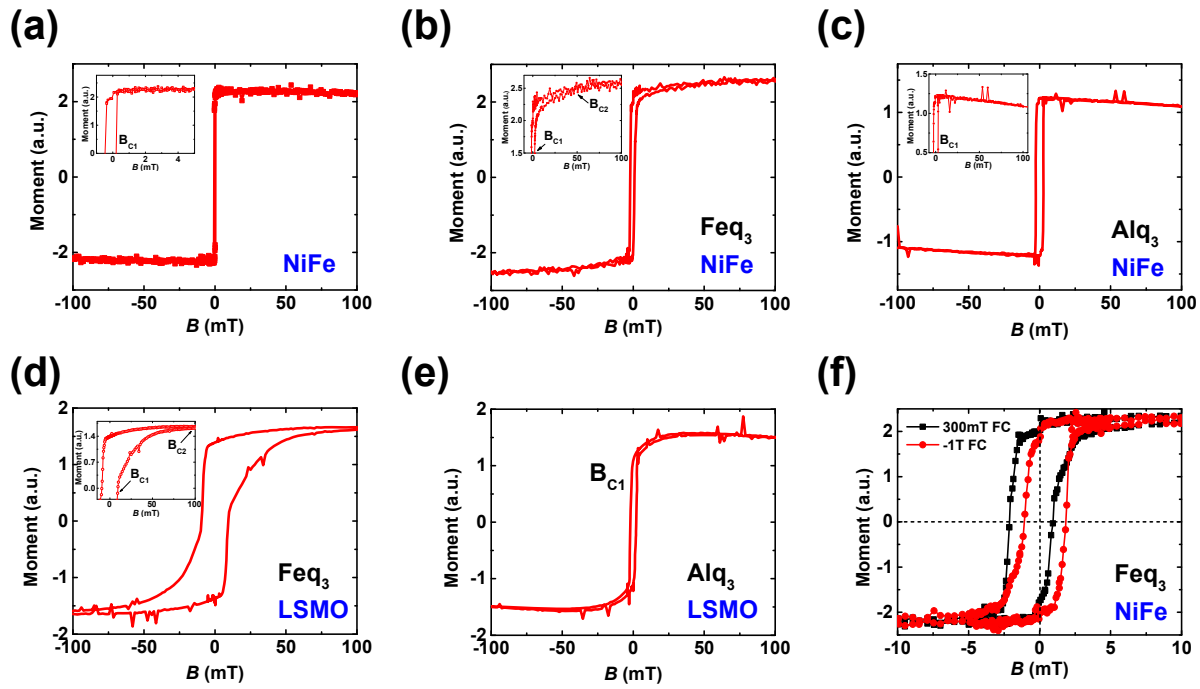

FIG. 3 (Color online) SQUID magnetometry of 'OSV-like' device structures. (a) to (e), *M(B)* response for NiFe, NiFe-Feq_3, NiFe-Alq_3, LSMO-Feq_3, and LSMO-Alq_3 structures, respectively, plotted up to ±100 mT. The insets in (a)-(c) magnify the *M*(*B*) response that exhibits additional hysteresis response of the deposited Feq_3 film onto the NiFe substrate. In panel (b**)**, the abrupt transition due to the FM substrate and broad transition from the Feq_3 layer are denoted as B_{C1} and B_{C2}, respectively, which is consistent with the MR(*B*) response in Fig. 2b. (f) *M(B)* responses of NiFe-Feq_3 that is cooled down under two different fields with opposite polarities, plotted up to ±10 mT. All *M*(*B*) measurements were performed at 5K.

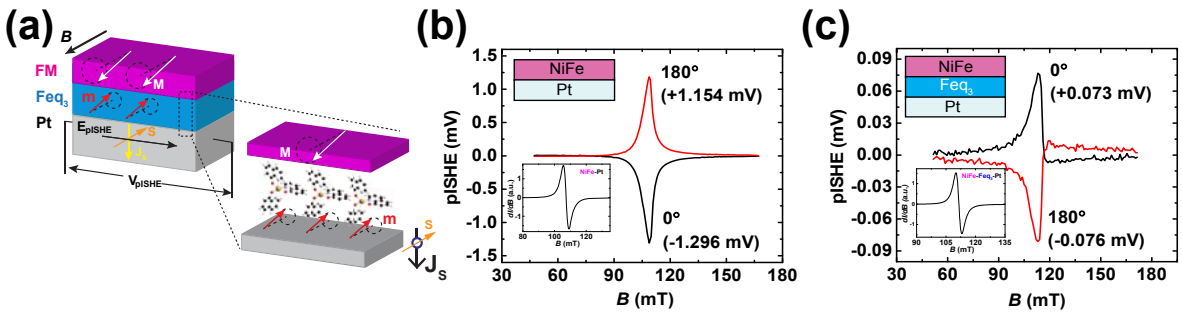

FIG. 4. (Color online) pulsed-ISHE(B) response in various Feq_3-based devices generated via spin-pumping. (a) Left panel: schematic illustration (not to scale) of the FM/Feq_3/Pt device. $\boldsymbol{B}$ and $\boldsymbol{M}$ denote, respectively, the static external magnetic field and dynamic magnetization in the FM film that precesses about $\boldsymbol{B}$. $\boldsymbol{J}_S$, $\boldsymbol{S}$, $\mathbf{E}_{ISHE}$, and $\mathbf{V}_{pISHE}$ denote, respectively, the flow of the pulsed spin current, spin polarization vector, generated electric field, and detected p-ISHE voltage. Right panel shows the magnetization precession of the Feq_3 layer, where $\boldsymbol{m}$ and derived $\boldsymbol{S}$ are antiparallel to $\boldsymbol{M}$, under the influence of FM layer via the AFM exchange interaction. (b) and (c) The respective $\mathbf{V}_{pISHE}(\boldsymbol{B})$ response of NiFe (15 nm)/Pt (10 nm) and NiFe (15 nm)/Feq_3 (7 nm)/Pt (10 nm), measured in device structures shown in the insets. All devices are capped with a SiO_2/Cu capacitor layer to suppress the anomalous Hall effect response component [51]. The black and red lines are for in-plane magnetic field $\boldsymbol{B}$ (at 0º) and $-\boldsymbol{B}$ (at 180º), respectively. The lower inset in each panel shows the appropriate FMR($\boldsymbol{B}$) response using the same device configuration.

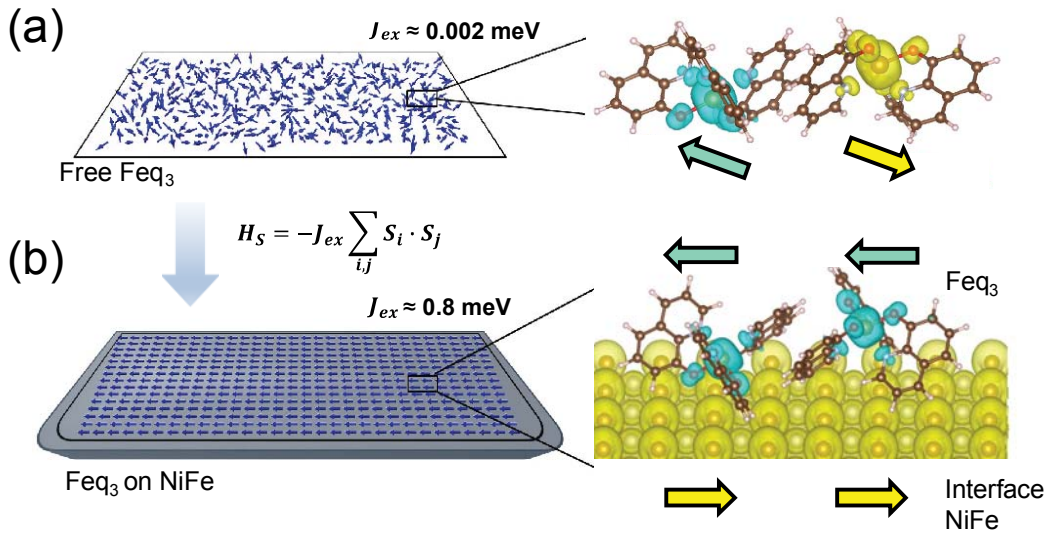

FIG. 5. (Color online) Theoretical DFT calculations. (a) and (b), the spin density of free Feq_3 molecules and Feq_3 in contact with the NiFe substrate, respectively. The effective coupling constant among the Feq_3 molecules in two systems are labeled, as deduced from Heisenberg spin lattice model. The small dark yellow and light yellow dots represent, respectively, the Fe and Ni atoms of NiFe at the interface. The yellow (blue) spheres denote spins oriented to the right (left side).